AMSE Association for the Advancement of Modelling & Simulation Techniques in Enterprises
IIETA International Information and Engineering Technology Association
Advancing the World of Information and Engineering

Modelling, Measurement and Control B
Vol. 87, No. 2, June, 2018, pp. 83-91
Journal homepage: http://iieta.org/Journals/MMC/MMC_B

Numerical analysis of non-Newtonian fluid in a non-Darcy porous channel

Funmilayo H. Oyelami[1*], Moses S. Dada[2]

[1] Department of Mathematical and Physical sciences, Afe Babalola University, Ado Ekiti 360001, Nigeria
[2] Department of Mathematics, University of Ilorin, Ilorin 240101, Nigeria

Corresponding Author Email: adefolajufunmilayo@gmail.com

https://doi.org/10.18280/mmc_b.870204

Received: 22 May 2018
Accepted: 27 June 2018

Keywords:
eyring-powell fluid, porous channel, darcy-forchheimer, crank-nicolson, unsteady

ABSTRACT

In this work, non-Newtonian fluid properties in a non-Darcy porous channel, specifically Darcy-Forchheimer porous channel is investigated with focus on a numerical analysis of Eyring-Powell type of non-Newtonian fluid. The unsteady state problem is considered under the influence of thermal radiation and transversely applied magnetic field. The governing non-linear partial differential equations were non-dimensionalized and then solved using Crank-Nicolson concept. Significance of non-Newtonian fluid properties as well as other fluid parameters is considered on the velocity, temperature and concentration profiles with the aid of graphs.

1. INTRODUCTION

Study of flow behaviour of non-Newtonian fluids in permeable medium is very essential due to the fact that non-Newtonian fluid demonstrate nonlinear relationship between shear stress and shear rate different from Newtonian fluids.

Eyring-Powell model is a very important type of rheological fluid model for analysing non-linear relationship between shear stress and rate of deformation. The Eyring-Powell type of rheological model modified after Manisha and Timol [1], Malik et al. [2] is given as

$$\tau_{xy} = \mu \frac{\partial u^*}{\partial y^*} + \frac{1}{a} sinh^{-1}\left(\frac{1}{c}\frac{\partial u^*}{\partial y^*}\right) \quad (1)$$

where μ, is the dynamic viscosity coefficient, a and c corresponds to Eyring-Powell parameters, $\frac{\partial u^*}{\partial y^*}$ stands for the rate of deformation, (x, y) are the Cartesian coordinates of any point in the flow domain and τ is the shear stress.

This model was discovered by Powell and Eyring [3].

When modelling flow of fluids in permeable channels, heat transfer analysis has always been of interest in controlling the rate of heat transfer, a better quality control in manufacturing industries and reduction in its emission to the body and its immediate environment. Adesanya and Gbadeyan [5], Islam et al. [6], Patel and Timol [7], Patel and Timol [8] and Hayat et al. [9], out of many researchers have greatly worked using this fluid model to describe non-linear behaviour of non-Newtonian fluids.

The Eyring-Powell model, according to Manisha and Timol [1], Khader and Megahed [10], Malik et al. [2], although more mathematically complex, has certain advantages over the Power-law fluid model. Eyring-Powell model works perfectly well for both low and high shear rate as it was based on the kinetic theory of liquids. Eldabe et al. [11] together with Zueco and Beg [12] investigated the Eyring-Powell fluid having the effect of couple stresses between two parallel plates.

Nabil et al. [13] studied heat and mass transfer MHD Eyring-Powell fluid with dissipation in a porous medium. In their work, the effects of thermal radiation were neglected. By using homotopy analysis, Malik et al. [2] obtained boundary layer Eyring-Powell fluid with a variable viscosity.

Over an exponentially shrinking sheet, Asmat et al. [14] examined radiation effects on boundary layer Eyring-Powell fluid using homotopy analysis. Tasawar et al. [15] using non-uniform heat source/sink investigated the Powell-Eyring fluid past an unsteady inclined stretching sheet. Darji and Timol [16] investigated the group theoretical similarity analysis for natural convection flow of some non-Newtonian fluid models. It was observed in their work that the velocity in Williamson model is higher than that of Prandtl-Eyring model.

Adesanya and Gbadeyan [5] employ Adomial decomposition method to study visco-elastic fluid flow having slip conditions. Gbadeyan and Dada [17] investigated heat transfer on an unsteady MHD Eyring-Powell fluid flow with slip in a porous medium.

In the above cited studies, attention has not been given to studies involving effects of thermal radiation, magnetic field and dissipation.

Oyelami and Dada [18] investigated an unsteady magnetohydrodynamic flow of both Prandtl-Eyring and Eyring-Powell non-Newtonian fluid model having slip through porous channel. Also, importance of magnetohydrodynamic Powell-Eyring fluid having thermal conductivity that is variable together with non-linear radiation over a porous cylinder was considered by Amit and Shalini [19].

The present study considered the effects of thermal radiation, magnetic field and dissipation on an unsteady MHD flow of non-Newtonian Eyring-Powell model. The equations governing the model were simplified, non-dimensionaliszd and solutions were provided by using Crank Nicolson finite difference method with the help of MATLAB programming package. Fluid parameters arising from the flow is shown graphically on velocity, temperature and concentration profiles.

2. PROBLEM FORMULATION

Unsteady incompressible and electrically conducting Eyring-Powell fluid is considered along a vertical plate in a porous medium. The x^* axis is taken in a vertically upward direction with y^*axis normal to it. Along y^*, a magnetic field of uniform strength is applied. It was initially assumed that at $t \leq 0$ both the plate and fluid maintain same temperature and concentration which are denoted by T_∞^* and C_∞^* respectively. Thereafter, temperature and concentration of the plate at $t > 0$ was raised and both maintained T_w^* and C_w^*. The fluid properties are assumed to be constant except that Boussinesq relations was used to approximate the body forces terms in the momentum equation. Taking into account viscous dissipation effects, radiative heat flux in the y^* direction is defined according to Modes [19] as follows:

$$q_r = -\frac{4\sigma \partial T^{*4}}{3k^1 \partial y^*} \tag{2}$$

The governing equations are

$$\frac{\partial u^*}{\partial x^*} + \frac{\partial v^*}{\partial y^*} = 0; \tag{3}$$

$$\frac{\partial u^*}{\partial t^*} + u^* \frac{\partial u^*}{\partial x^*} + v^* \frac{\partial u^*}{\partial y^*} = \frac{1}{\rho}\frac{\partial}{\partial y^*}(\tau_{xy}) + g\beta_T(T^* - T_\infty^*) + g\beta_c(C^* - C_\infty^*) - \frac{\sigma B_0^2 u^*}{\rho} - \frac{\nu u^*}{k} - \frac{b u^{*2}}{k} \tag{4}$$

$$\frac{\partial T^*}{\partial t^*} + u^* \frac{\partial T^*}{\partial x^*} + v^* \frac{\partial T^*}{\partial y^*} = \alpha \frac{\partial^2 T^*}{\partial y^{*2}} - \frac{1}{\rho C_p}\frac{\partial q_r}{\partial y^*} + \frac{\nu}{C_p}\left(\frac{\partial u^*}{\partial y^*}\right)^2 \tag{5}$$

$$\frac{\partial C^*}{\partial t^*} + u^* \frac{\partial C^*}{\partial x^*} + v^* \frac{\partial C^*}{\partial y^*} = D \frac{\partial^2 C^*}{\partial y^{*2}} - K_c(C^* - C_\infty^*) \tag{6}$$

with the following as the initial and boundary conditions:

$$\begin{aligned} &t^* \leq 0: u^* = 0, v^* = 0, T^* = T_\infty^*, C^* \\ &\qquad = C_\infty^* \quad for\ every\ x^*\ and\ y^* \\ &t^* > 0: u^* = u_o^*, v^* = 0, T^* = T_w^*, \quad C^* = C_w^* \quad at\ y^* = 0 \\ &u^* = 0, T^* = T_\infty^*, C^* = C_\infty^* \quad at\ x^* = 0 \\ &u^* \to 0, T^* \to T_\infty^*, C^* \to C_\infty^* \quad as\ y^* \to \infty. \end{aligned} \tag{7}$$

where u^* and v^* implies the velocities in x^* and y^* directions, T^* and C^* are fluid temperature and concentration of the fluid, $\rho, g, t, \beta_T, \beta_C, \sigma, k, b, D, C_p, \alpha, B_o, K_c, q_r, \nu,$

τ_{xy} are density, gravitational acceleration, time, thermal volumetric coefficient, concentration volumetric coefficient, electric conductivity, permeability, Darcy-Forchheimer, concentration diffusivity, specific heat at constant pressure, thermal diffusivity, magnetic field, chemical reaction, radiative heat flux, kinematic viscosity and stress tensor parameters respectively.

From equation (1), Eyring-Powell non-Newtonian fluid model modified after Manisha and Timol [1], Malik et al. [2] is expressed as

$$\tau_{xy} = \mu \frac{\partial u^*}{\partial y^*} + \frac{1}{a} sinh^{-1}\left(\frac{1}{c}\frac{\partial u^*}{\partial y^*}\right) \tag{8}$$

where the first and second term in the series expansion of

$$\sin h^{-1}\left(\frac{1}{c}\frac{\partial u^*}{\partial y^*}\right) \cong \frac{1}{c}\frac{\partial u^*}{\partial y^*} - \frac{1}{6}\left(\frac{1}{c}\frac{\partial u^*}{\partial y^*}\right)^3, \left|\frac{1}{c}\frac{\partial u^*}{\partial y^*}\right| \ll 1 \tag{9}$$

substituting equation (9) into equation (8),

$$\tau_{xy} = \mu \frac{\partial u^*}{\partial y^*} + \frac{1}{ac}\frac{\partial u^*}{\partial y^*} - \frac{1}{6a}\left(\frac{1}{c}\frac{\partial u^*}{\partial y^*}\right)^3 \tag{10}$$

This study concerns an optically thick limit boundary layers. If there are sufficiently small temperature differences within the flow, then expressing quartic temperature function as a linear function of temperature according to Raptis and Perdikis [20], the Taylor series for T^{*4} ignoring terms of higher order can be written as:

$$T^{*4} \approx 4T_\infty^{*3} - 3T_\infty^{*4} \tag{11}$$

Substituting equation (11) into (2) yields the following result for energy equation

$$\frac{\partial T^*}{\partial t^*} + u\frac{\partial T^*}{\partial x} + v\frac{\partial T^*}{\partial y} = \alpha \frac{\partial^2 T^*}{\partial y^{*2}} + \frac{\nu}{\rho C_p}\left(\frac{\partial u^*}{\partial y^*}\right)^2 + \frac{16\sigma T_\infty^{*3}}{3k^1 \rho c_p}\frac{\partial^2 T^*}{\partial y^{*2}} \tag{12}$$

Hence, the governing dimensional equations becomes

$$\frac{\partial u^*}{\partial x^*} + \frac{\partial v^*}{\partial y^*} = 0; \tag{13}$$

$$\frac{\partial u^*}{\partial t^*} + u^* \frac{\partial u^*}{\partial x^*} + v^* \frac{\partial u^*}{\partial y^*} = \frac{1}{\rho}\frac{\partial}{\partial y^*}\left[\mu \frac{\partial u^*}{\partial y^*} + \frac{1}{ac}\frac{\partial u^*}{\partial y^*} - \frac{1}{6a}\left(\frac{1}{c}\frac{\partial u^*}{\partial y^*}\right)^3\right] + g\beta_T(T^* - T_\infty^*) + g\beta_c(C^* - C_\infty^*) - \frac{\sigma B_0^2 u^*}{\rho} - \frac{\nu u^*}{k} - \frac{b u^{*2}}{k} \tag{14}$$

$$\frac{\partial T^*}{\partial t^*} + u\frac{\partial T^*}{\partial x} + v\frac{\partial T^*}{\partial y} = \alpha \frac{\partial^2 T^*}{\partial y^{*2}} + \frac{\nu}{\rho C_p}\left(\frac{\partial u^*}{\partial y^*}\right)^2 + \frac{16\sigma T_\infty^{*3}}{3k^1 \rho c_p}\frac{\partial^2 T^*}{\partial y^{*2}} \tag{15}$$

$$\frac{\partial C^*}{\partial t^*} + u^* \frac{\partial C^*}{\partial x^*} + v^* \frac{\partial C^*}{\partial y^*} = D \frac{\partial^2 C^*}{\partial y^{*2}} - K_c(C^* - C_\infty^*) \tag{16}$$

Transforming the dimensional governing equations (13), (14), (15) and (16) with the following non-dimensional quantities

$$X = \frac{x^* u_0^*}{\nu}, Y = \frac{y^* u_0^*}{\nu}, U = \frac{u^*}{u_0^*}, t = \frac{t^* u_0^{*2}}{\nu}, T = \frac{T^* - T_\infty^*}{T_w^* - T_\infty^*}, C = \frac{C^* - C_\infty^*}{C_w^* - C_\infty^*}, Re = \frac{u_0^* l}{\nu}, Ec = \frac{u_0^{*2}}{C_p(T_w^* - T_\infty^*)}, Pr = \frac{\nu}{\alpha}, M = \frac{\sigma B_0^2 \upsilon}{\rho u_0^{*2}}, \mathrm{A} = \frac{1}{a\mu c}, Sc = \frac{\nu}{\alpha}, Da = \frac{k}{l^2}, R = \frac{k^1 k}{4\sigma T_\infty^{*3}}, Gr = \frac{g\beta_T(T_w^* - T_\infty^*)}{u_0^{*3}}, Gm = \frac{g\beta_c(C_w^* - C_\infty^*)}{u_0^{*3}}, \mathrm{F} = \frac{u_0^{*4}}{2\rho a \nu^3 c^3}, \gamma = \frac{K_c h^2}{\upsilon} \tag{17}$$

Gives the following set of non-dimensional equations

$$\frac{\partial U}{\partial X} + \frac{\partial V}{\partial Y} = 0 \tag{18}$$

$$\frac{\partial U}{\partial t} + U\frac{\partial U}{\partial X} + V\frac{\partial U}{\partial Y} = \left[1 + A - F\left(\frac{\partial U}{\partial Y}\right)^2\right]\frac{\partial^2 U}{\partial Y^2} + GrT + GmC - MU - \frac{U}{DaRe^2} - \frac{FsU^2}{DaRe} \tag{19}$$

$$\frac{\partial T}{\partial t} + U\frac{\partial T}{\partial X} + V\frac{\partial T}{\partial Y} = \frac{1}{Pr}\left(1 + \frac{4}{3N}\right)\frac{\partial^2 T}{\partial Y^2} + Ec\left(\frac{\partial U}{\partial Y}\right)^2 \tag{20}$$

$$\frac{\partial C}{\partial t} + U\frac{\partial C}{\partial X} + V\frac{\partial C}{\partial Y} = \frac{1}{Sc}\frac{\partial^2 C}{\partial Y^2} - \gamma C \tag{21}$$

with the following as non-dimensional initial and boundary conditions

$t \leq 0$:
$U = 0, V = 0, T = 0, C = 0 \forall X \; and \; Y$
$t > 0$:
$U = 1, V = 0, T = 1, C = 1 at \; Y = 0$
$U = 0, T = 0, C = 0, at \; X = 0$
$\mathrm{U} \rightarrow 0, T \rightarrow 0, \quad C \rightarrow 0 \; as \; Y \rightarrow \infty$ (22)

where T implies the non-dimensional temperature, C denotes the non-dimensional concentration, Da implies the Darcy number, Gr and Gm stands for thermal and modified Grashof numbers respectively, N stands for thermal radiation parameter, Fs denotes the Darcy -Forchheimer inertia number, Pr is the Prandtl number, γ stands for chemical reaction parameter, Sc implies the Schimdt number, Re stands for Reynold number, U and V denotes dimensionless velocities in X and Y directions, A and F are the properties of Eyring-Powell parameter.

3. SOLUTION METHOD

Solution to this problem is carried out using Crank-Nicolson implicit finite difference approach. The corresponding finite difference equations to the non- dimensional governing equations (18), (19), (20) and (21) under (22) are given as:

$$\frac{U_{i,j}^{k+1}-U_{i-1,j}^{k+1}+U_{i,j}^{k}-U_{i-1,j}^{k}+U_{i,j-1}^{k+1}-U_{i-1,j-1}^{k+1}+U_{i,j-1}^{k}-U_{i-1,j-1}^{k}}{4\Delta X}+\frac{V_{i,j}^{k+1}-V_{i,j-1}^{k+1}+V_{i,j}^{k}-V_{i,j-1}^{k}}{2\Delta Y}=0 \quad (23)$$

$$\frac{U_{i,j}^{k+1}-U_{i,j}^{k}}{\Delta t}+U_{i,j}^{k}\frac{\left(U_{i,j}^{k+1}-U_{i-1,j}^{k+1}+U_{i,j}^{k}-U_{i-1,j}^{k}\right)}{2\Delta X}+V_{i,j}^{k}\frac{\left(U_{i,j+1}^{k+1}-U_{i,j-1}^{k+1}+U_{i,j+1}^{k}-U_{i,j-1}^{k}\right)}{4\Delta Y}=\left[1+A-F\left(\frac{u_{j+1}^{k}-u_{j-1}^{k}}{2\Delta y}\right)^{2}\right]\frac{U_{i,j-1}^{k+1}-2U_{i,j}^{k+1}+U_{i,j+1}^{k+1}+U_{i,j-1}^{k}-U_{i,j}^{k}+U_{i,j+1}^{k}}{2(\Delta Y)^{2}}-\frac{1}{2DaRe^{2}}\left(U_{i,j}^{k+1}+U_{i,j}^{k}\right)-\frac{FsU_{i,j}^{k}}{2DaRe}\left(U_{i,j}^{k+1}+U_{i,j}^{k}\right)+\frac{Gr}{2}\left(T_{i,j}^{k+1}+T_{i,j}^{k}\right)+\frac{Gm}{2}\left(C_{i,j}^{k+1}+C_{i,j}^{k}\right)-\frac{M}{2}\left(U_{i,j}^{k+1}+U_{i,j}^{k}\right) \quad (24)$$

$$\frac{T_{i,j}^{k+1}-T_{i,j}^{k}}{\Delta t}+U_{i,j}^{k}\frac{\left(T_{i,j}^{k+1}-T_{i-1,j}^{k+1}+T_{i,j}^{k}-T_{i-1,j}^{k}\right)}{2\Delta X}+V_{i,j}^{k}\frac{\left(T_{i,j+1}^{k+1}-T_{i,j-1}^{k+1}+T_{i,j+1}^{k}-T_{i,j-1}^{k}\right)}{4\Delta Y}=\frac{1}{Pr}\left(1+\frac{4}{3N}\right)\frac{T_{i,j-1}^{k+1}-2T_{i,j}^{k+1}+T_{i,j+1}^{k+1}+T_{i,j-1}^{k}-T_{i,j}^{k}+T_{i,j+1}^{k}}{2(\Delta Y)^{2}}+Ec\left(\frac{U_{i,j+1}^{k}-U_{i,j-1}^{k}}{2\Delta Y}\right)^{2} \quad (25)$$

$$\frac{C_{i,j}^{k+1}-C_{i,j}^{k}}{\Delta t}+U_{i,j}^{k}\frac{\left(C_{i,j}^{k+1}-C_{i-1,j}^{k+1}+C_{i,j}^{k}-C_{i-1,j}^{k}\right)}{2\Delta X}+V_{i,j}^{k}\frac{\left(C_{i,j+1}^{k+1}-C_{i,j-1}^{k+1}+C_{i,j+1}^{k}-C_{i,j-1}^{k}\right)}{4\Delta Y}=\frac{1}{Sc}\frac{C_{i,j-1}^{k+1}-2C_{i,j}^{k+1}+C_{i,j+1}^{k+1}+C_{i,j-1}^{k}-C_{i,j}^{k}+C_{i,j+1}^{k}}{2(\Delta Y)^{2}}-\frac{\gamma}{2}\left(C_{i,j}^{k+1}+C_{i,j}^{k}\right) \quad (26)$$

multiplying equations (23), (24), (25) and (26) by Δt for simplicity, the equations are arranged so that velocities, temperature and concentration involving present time step (k+1) are on the left while those of previous time step (k) are on the right hand side. Hence, the equations form tri-diagonal matrix system. The finite difference equations (23), (24), (25) and (26) in tridiagonal matrix system of equation is as follows:

$$-V_{i,j-1}^{k+1}+V_{i,j}^{k}=F_1 \quad (27)$$

$$-A_2U_{i,j-1}^{k+1}+B_2U_{i,j}^{k+1}+D_2U_{i,j+1}^{k+1}=F_2 \quad (28)$$

$$-A_3T_{i,j-1}^{k+1}+B_3T_{i,j}^{k+1}+D_3T_{i,j+1}^{k+1}=F_3 \quad (29)$$

$$-A_4C_{i,j-1}^{k+1}+B_4C_{i,j}^{k+1}+D_4C_{i,j+1}^{k+1}=F_4 \quad (30)$$

where

$$A_2=E_3+E_6, B_2=1+E_2+2E_6+E_7+E_8+E_9+E_{10}, D_2=E_3-E_6$$
$$A_3=E_3+E_{10}, B_3=1+E_2+2E_{10}, D_3=E_3-E_{10}$$
$$A_4=E_3+E_{12}, B_4=1+E_2+2E_{12}+E_{13}, D_4=E_3-E_{12} \quad (31)$$

And

$$F_1=E_1\begin{bmatrix}U_{i,j}^{k+1}-U_{i-1,j}^{k+1}+U_{i,j}^{k}-U_{i-1,j}^{k}\\+U_{i,j-1}^{k+1}-U_{i-1,j-1}^{k+1}+U_{i,j-1}^{k}-\\U_{i-1,j-1}^{k}\end{bmatrix}+V_{i,j-1}^{k+1}-V_{i,j}^{k} \quad (32)$$

$$F_2=(E_3+E_6)U_{i,j-1}^{k}+(1-E_2-2E_6-E_7-E_8-E_9-E_{10})U_{i,j}^{k}-(E_3-E_6)U_{i,j+1}^{k}+E_4\left[T_{i,j}^{k+1}+T_{i,j}^{k}\right]+E_5\left[C_{i,j}^{k+1}+C_{i,j}^{k}\right]+E_2U_{i-1,j}^{k+1}+E_2U_{i-1,j}^{k} \quad (33)$$

$$F_3=(E_3+E_{10})T_{i,j-1}^{k}+(1-E_2-2E_{10})T_{i,j}^{k}-(E_3-E_{10})T_{i,j+1}^{k}+E_2T_{i-1,j}^{k+1}+E_2T_{i-1,j}^{k}+E_{11}\left[U_{i,j+1}^{k}-U_{i,j-1}^{k}\right]^{2} \quad (34)$$

$$F_4=(E_3+E_{12})C_{i,j-1}^{k}+(1-E_2-2E_{12}-E_{13})C_{i,j}^{k}-(E_3-E_{12})C_{i,j+1}^{k}+E_2C_{i-1,j}^{k+1}+E_2C_{i-1,j}^{k} \quad (35)$$

Also

$$E_1=-\frac{\Delta Y}{2\Delta X}, E_2=\frac{\Delta t}{2\Delta X}U_{i,j}^{k}, E_3=\frac{\Delta t}{4\Delta Y}V_{i,j}^{k}, E_4=\frac{\Delta tGr}{2}, E_5=\frac{\Delta tGm}{2} E_6=\frac{H_i\Delta t}{2(\Delta Y)^{2}}, E_7=\frac{\Delta t}{2DaRe^{2}}, E_8=\frac{\Delta tFs}{2DaRe} U_{i,j}^{k}, E_9=\frac{\Delta tM}{2}, E_{10}=\frac{1}{Pr}\left[1+\frac{4}{3N}\right]\frac{\Delta t}{2(\Delta Y)^{2}}, E_{11}=\frac{\Delta t}{4(\Delta Y)^{2}}Ec, E_{12}=\frac{\Delta t\gamma}{2}, H_i=\left[1+A-F\left(\frac{u_{j+1}^{k}-u_{j-1}^{k}}{2\Delta y}\right)^{2}\right] \quad (36)$$

Along X direction is defined a grid point i while j and k are the grid points along Y and t directions. Dividing X and Y into M and N grid gave a well-spaced points. Mesh sizes were taken to be ΔX=0.05, ΔY=0.25 and Δt=0.01 and a rectangle with maximum value for X = 1.05 and maximum value for Y=5.25 while Ymax lie outside the boundary layers of momentum, energy and concentration.

At a particular time during computations, the coefficients $U_{i,j}^{k}$ and $V_{i,j}^{k}$ in the finite difference equation were taken to be constants. From the initial conditions at all grid points, the

values of C, T, U and V are known. For the calculations of C, T, U and V at present time (k+1), the known values at previous time level (k) are used as follows:

The tri-diagonal system of equations (30) appearing at every internal nodal point particularly on a i – level was solved using Thomas algorithm. The solution provided helps in the computation of Concentration (C) values particularly on a i – level at time (k+1) at every nodal point. The same procedure used to compute C values using equation (30) was repeated for Tri diagonal system of equations (29) to compute the values for temperature (T) at time (k+1) level. The results gotten from the computations of concentration (C) and Temperature (T) at time (k+1) level are used in equation (28) to compute the values of velocity (U) at time (k+1) level.

By so doing, computations of values for C, T and U are known on a particular i – level and the procedure was repeated severally at various i – levels. This approach gave the values of C, T and U at all grid point.

The computation of values for V is carried out explicitly at every nodal point using equation (27) on a particular i – level at time (k+1).

4. DISCUSSION OF RESULTS

Computation is conducted to examine the influence of fluid parameters graphically on velocity, temperature and concentration profiles. Default values are given as: A =2, F =0.5, Gr=2, Gm=2, M=2, γ=1 , Da=0.2, Fs=0.2 Re=1, Pr=1.0, N=3.0, Ec=0.002, Sc=1.0 and all graph corresponds to these values except otherwise stated. To check the correctness of this work, it was compared with the Newtonian work of Anwar et al. (2008) by setting the non-Newtonian parameters to zero and it was found to be in good agreement as seen in figure 1.

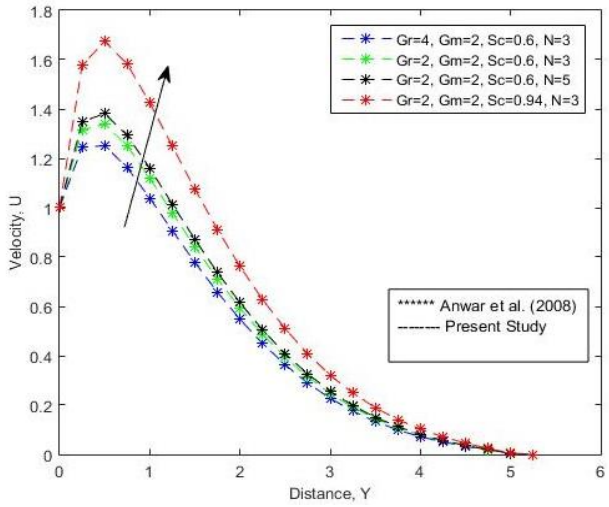

Figure 1. Velocity profile for various values of Gr, Gm, Sc and N at A=F=0

Figures 2, 3 and 4 display the influence of magnetic field parameters on fluid velocity, temperature and concentration profiles respectively. A rise in magnetic field values causes velocity profile to decrease. The reduction experienced is as a result of the presence of Lorentz force with its power exerting force that reduces the motion of the fluid. Temperature and concentration distribution was seen to increase with increase in magnetic field in figures 3 and 4 respectively.

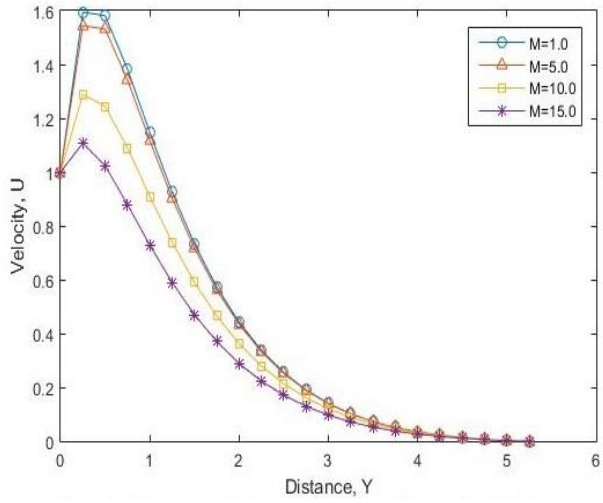

Figure 2. Velocity profile for various values of magnetic field parameter

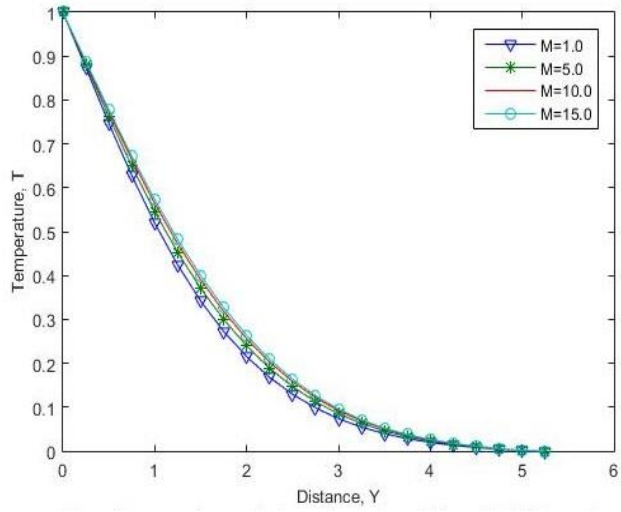

Figure 3. Temperature profile for various values of magnetic field parameter

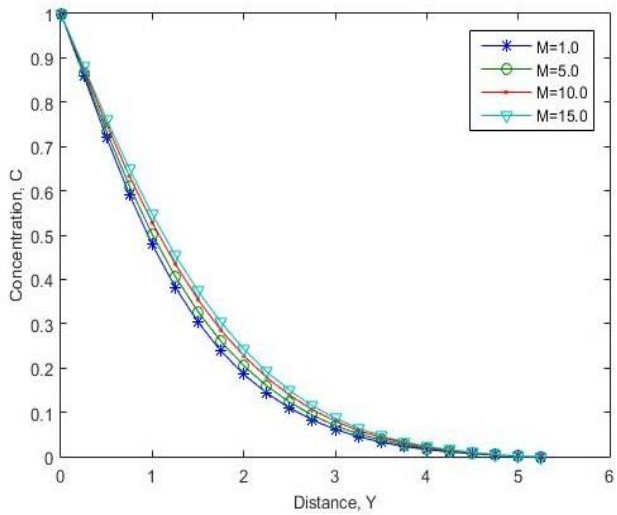

Figure 4. Concentration profile for various values of magnetic field parameter

The influence of increasing thermal radiation values N on velocity distribution is presented in figure 5. A rise in N

reduces velocity profile which is therefore accompanied by reduction in momentum boundary layers. Figures 6 and 7 display the temperature and concentration fields for various radiation parameter N. These plots show a decrease in temperature profile as N increases and an increase in the fluid concentration as thermal radiation increases in figures 6 and 7 respectively. This is because with higher values of N, smaller radiation flux is experienced and the rate at which energy is being transported to the fluid decreases.

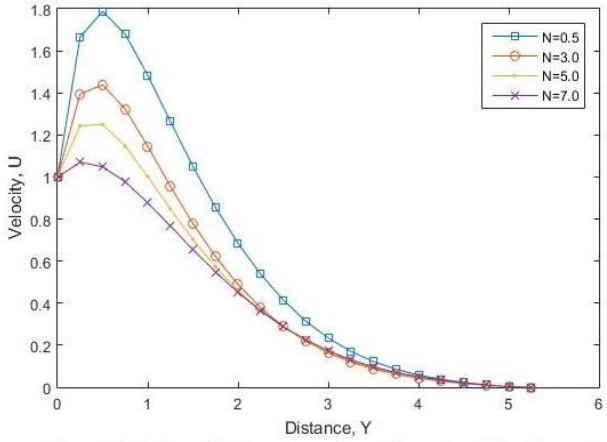

Figure 5. Velocity profile for various values ofthermal radiation parameter

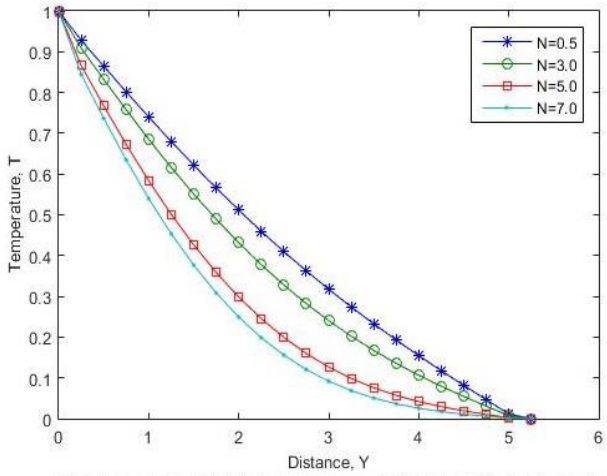

Figure 6. Temperature profile for various values of thermal radiation parameter

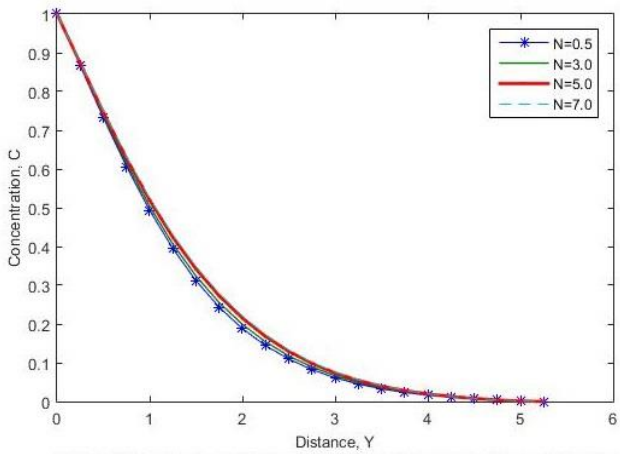

Figure 7. Concentration profile for various values of thermal radiation parameter

Figure 8, 9 and 10 represents the effects of Schmidt number Sc on the velocity, temperature and concentration distributions respectively. Velocity and concentration decreases as a result of increase in Schmidt number which causes a reduction in velocity, diffusivity and the concentration boundary layer thickness. This is because the thickness ratio for the viscous and concentration boundary layer is measured by Schmidt number. With larger Sc, low diffusion property is experienced which implies that concentration boundary layer becomes thinner than the velocity boundary layer thickness in the fluid. An Increase in Schmidt number amounts to slight increases in the fluid temperature.

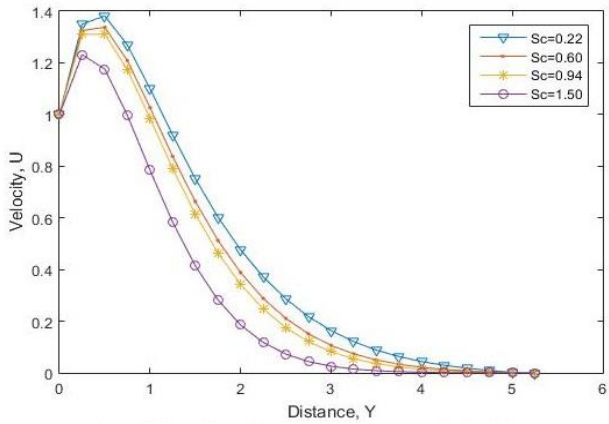

Figure 8. Velocity profile for various values of Schmidt number

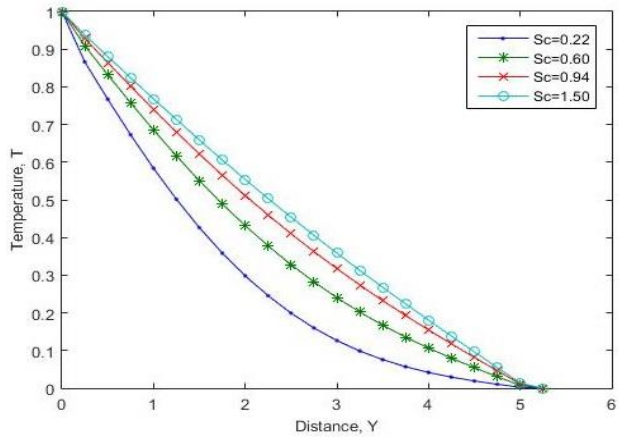

Figure 9. Temperature profile for various values of Schmidt number

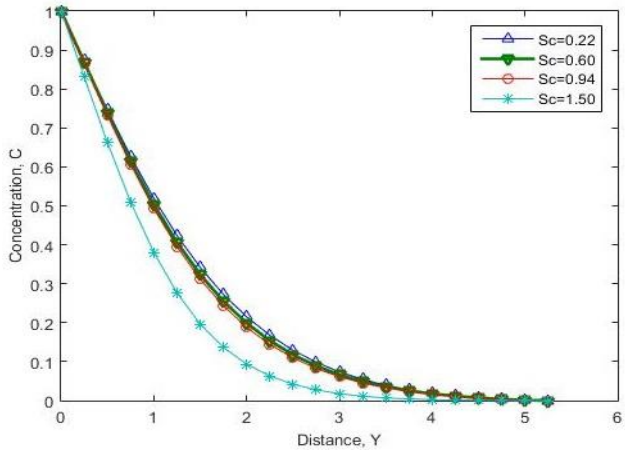

Figure 10. Concentration profile for various values of Schmidt number

Figure 11 shows the influence of thermal Grashof number Gr on the velocity profile. With a rise in Gr, velocity profile experienced an increase and this increase boosts the buoyancy force with an increase in the wall velocity and smoothly descends towards zero.

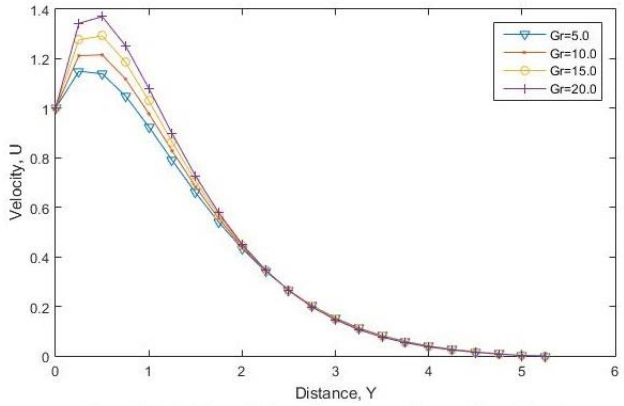

Figure 11. Velocity profile for various values of thermal Grashof number

Figure 12 presents temperature profile for thermal Grashof number Gr. Temperature profile smoothly decreases from 1 at the peak down the free stream. Concentration of the fluid also decreases down the stream as shown on figure 13.

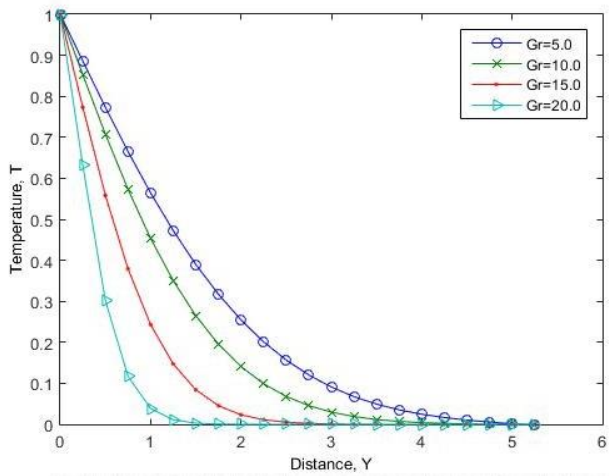

Figure 12. Temperature profile for various values of thermal Grashof number

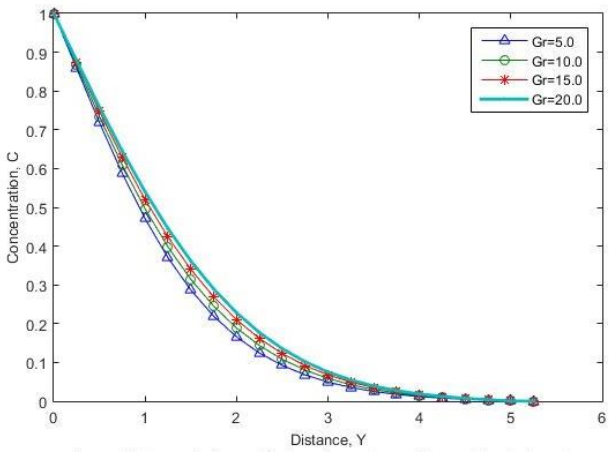

Figure 13. Concentration profile for various values of thermal Grashof number

Figures 14 and 15 illustrate the importance of modified Grashof number Gm on the distribution of velocity and temperature respectively. Effect of modified Grashof number Gm on the velocity profile is seen to accelerate the magnitude of velocity. This is as a result of its property which gives the relative importance of buoyancy force to the viscous forces. Increasing Gm amounts to a decreased temperature field and increased velocity field down the free stream.

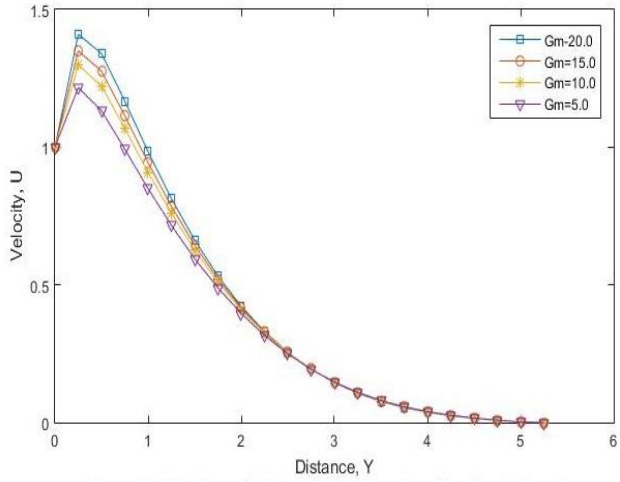

Figure 14. Velocity profile for various values of modified Grashof number

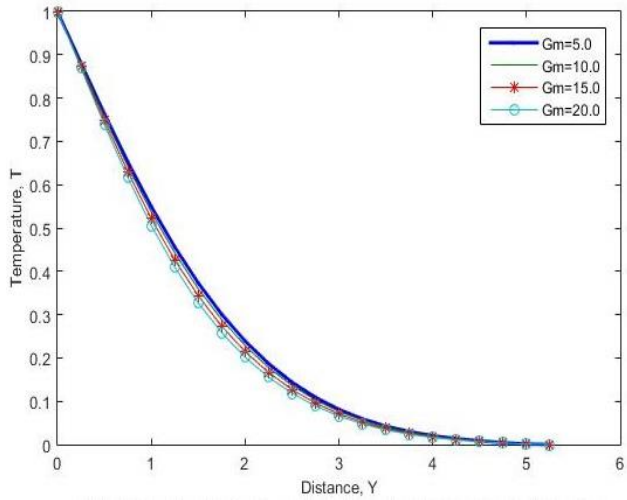

Figure 15. Temperature profile for various values of modified Grashof number

Figures 16 and 17 depict various Prandtl number Pr values on velocity and temperature fields respectively. Pr is the ratio of momentum diffusivity to thermal diffusivity. A rise in Pr numbers decreases significantly the velocity and temperature profiles. This is because smaller values of Pr increases the thermal conductivity of the fluid which indicates that heat is able to diffuse away from the heated surface more rapidly than higher values of Pr and temperatures across the boundary layer reduces more for higher Pr values.

Figures 18 and 19 show the influence of Eckert number on the velocity and temperature profiles. Increasing Eckert number causes a reduction in both the velocity and temperature profiles with significant changes in the momentum and thermal boundary layer thicknesses.

Figure 20 represents the velocity profile for non-Newtonian fluid parameter A. Parameter A causes a retarding effect on

the rate of flow and thereby reduces the fluid velocity giving significant changes in the momentum boundary layer thickness. Figure 21 exhibits the influence of the non-Newtonian Parameter F on the velocity field. It was observed that increasing F causes the fluid velocity to increase.

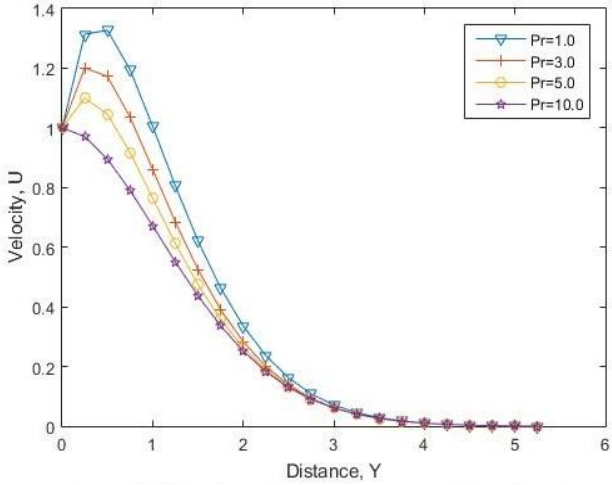

Figure 16. Velocity profile for various values of Prandtl number

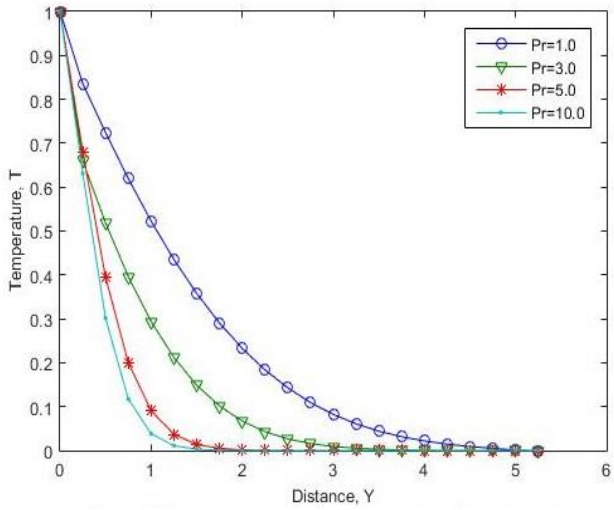

Figure 17. Temperature profile for various values of Prandtl number

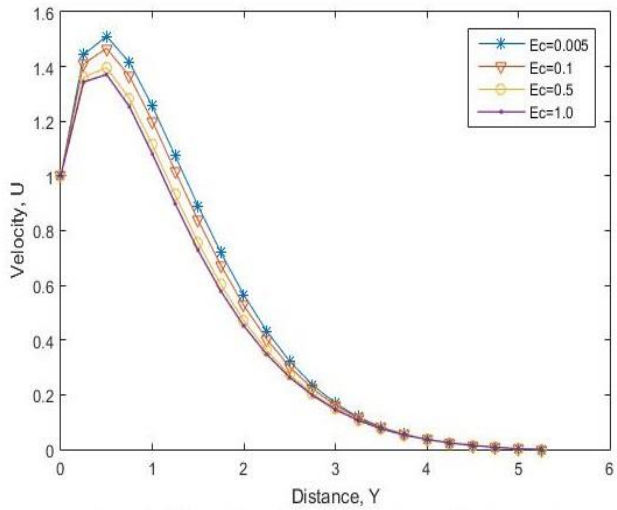

Figure 18. Velocity profile for various values of Eckert number

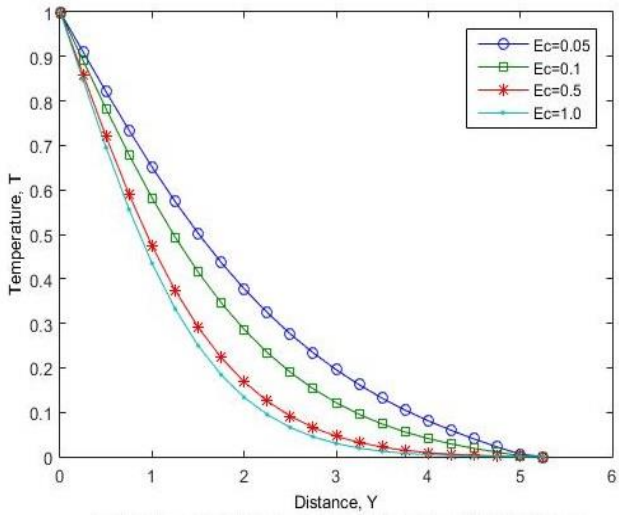

Figure 19. Temperature profile for various values of Eckert number

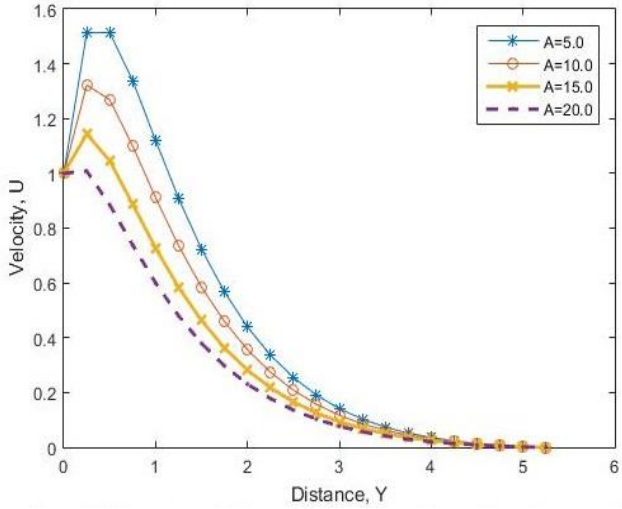

Figure 20. Velocity profile for various values of Eyring-Powell parameter A

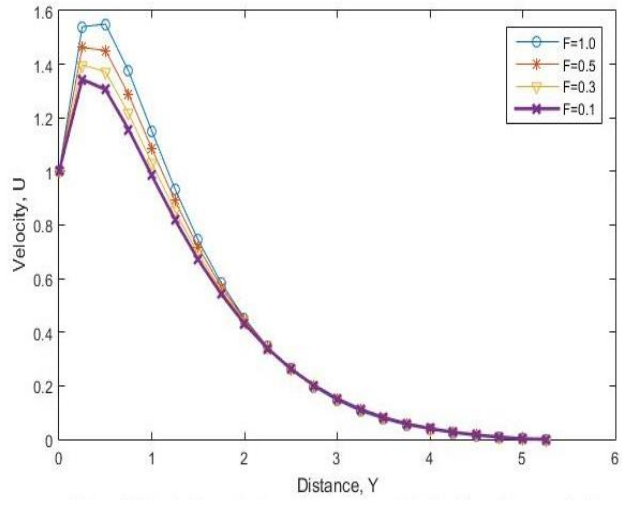

Figure 21. Velocity profile for various values of Eyring-Powell parameter F

The variations of velocity and temperature with Darcy-Forchheimer number Fs are presented on figures 22 and 23 respectively. As Fs increases, an increase in the fluid temperature and a reduction in the velocity of the fluid was experienced because increasing permeability increases the flow resistance reducing the fluid velocity and increasing its temperature.

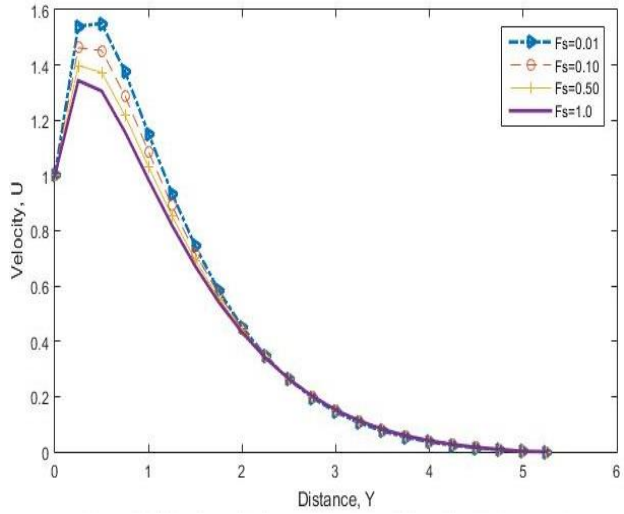

Figure 22. Velocity profile for various values of Darcy-Forchheimer number

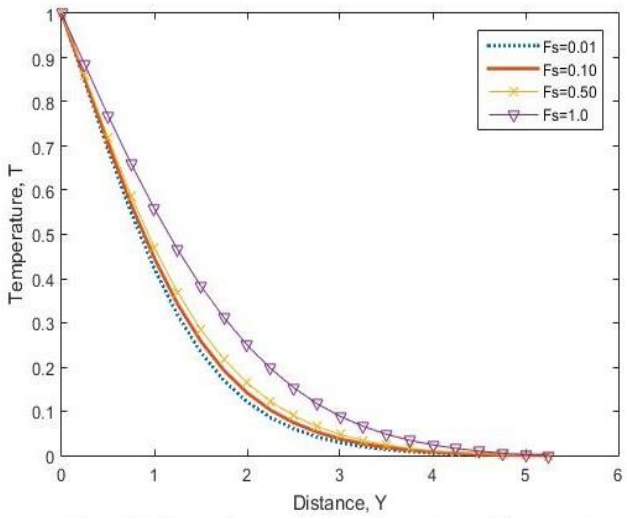

Figure 23. Temperature profile for various values of Darcy-Forchheimer number

5. CONCLUSION

In this work, non-Newtonian fluid properties in a Darcy-Forchheimer porous medium is investigated with focus on a numerical analysis of Eyring-Powell flow. The unsteady state problem is considered under the influence of thermal radiation and transversely applied magnetic field. The equations governing the problem were non-dimensionalzed and solved using Crank-Nicolson concept with MATLAB Programming package. The study revealed that increasing thermal Grashof number, non-Newtonian Parameter F and modified Grashof number Gm causes an increase in velocity distribution while velocity was reduced with a rise in magnetic field parameter,Eckert number, Schmidt number, non-Newtonian Parameter A, thermal radiation parameter, Darcy-Forchheimer number and Prandtl Number. Temperature rises as Schmidt number and magnetic field increases while it decreases as Prandtl number, thermal Grashof number, modified Grashof number, thermal radiation number and viscous dissipation parameter increases. Increasing thermal Grashof number, Schmidt number and magnetic field causes a decrease in concentration profile.

REFERENCES

[1] Manisha P, Timol MG. (2009). Numerical treatment of powell-eyring fluid flow using method of satisfaction of asymptotic boundary conditions. Journal of Applied Numerical Mathematics 59: 2584-2592. https://doi.org/10.1016/j.apnum.2009.04.010

[2] Malik MY, Hussian A, Nadeems. (2013). Boundary layer flow of an Eyring-Powell model fluid due to a stretching cylinder with variable viscosity. Journal of Scientia Iranica 20(2): 313-321. https://doi.org/10.1016/j.scient.2013.02.028

[3] Powell RE, Eyring H. (1944). Mechanism for relaxation theory of viscosity. Nature 154: 427-428.

[4] Bird RB, Stewart WE, Lightfoot EM. (1960). Transport phenomena. John Wiley, New York.

[5] Adesanya SO, Gbadeyan JA. (2011). Adomian Decomposition approach to steady visco-elastic flow with slip through a planar channel. Journal of Nonlinear Science 11(1): 86-94.

[6] Islam S, Shah A, Zhou CY, Ali I. (2009). Homotopy pertubation analysis of slider bearing with Powell-Eyring fluid. Z. Angew. Math. Phys. 60: 178-1193. https://doi.org/10.1007/s00033-009-7034-9

[7] Patel M, Timol MG. (2009). Numerical treatment of Powell Eyring fluid flow using method of asymptotic boundary conditions. Appl. Numer. Math. 59: 2584-2592. https://doi.org/10.1016/j.apnum.2009.04.010

[8] Patel M, Timol MG. (2011). Numerical treatment of MHD Powell Eyring fluid flow using method of satisfaction of asymptotic boundary conditions. Int. J. Math. Sci. Comput. 2: 71-78.

[9] Hayat T, Iqbal Z, Qasim M, Obaidat S. (2012). Steady flow of an Eyring Powell fluid over a moving surface with convective boundary conditions. Int. J. Heat Mass Transfer 55: 1817-1822. https://doi.org/10.1016/j.ijheatmasstransfer.2011.10.046

[10] Khader MM, Megahed AM. (2013). Numerical studies for flow and heat transfer of the Powell-Eyring fluid thin film over an unsteady stretching sheet with internal heat generation using the finite difference method. Journal of Applied Mechanics Technical Phys. 5(4): 440-450. https://doi.org/10.1134/S0021894413030139

[11] Eldaebe NTM, Hassan AA, Mona AA. (2003). Effect of couple stresses on the MHD of a non-Newtonian unsteady flow between two parallel porous plates. Journal of physics 58a: 204-210.

[12] Zueco J, Beg OA. (2009). Network numerical simulation applied to pulsatile non-Newtonian flow through a channel with couple stress and wall mass effects. International Journal of Applied Mathematics and Mech. 5: 1-16.

[13] Eldabe NTM, Sallam N, Sallam Mohamed Y, Abou-zeid (2012). Numerical study of viscous dissipation effect on

free convection heat and mass transfer of MHD non-Newtonian fluid flow through a porous medium. Journal of the Egyptian Mathematical Society 20: 139-151. https://doi.org/10.1016/j.joems.2012.08.013

[14] Ara A, Khan NA, Khan H, Sultan F. (2014). Radiation effects on boundary layer flow of an Eyring-Powell fluid over an exindent potentially shrinking sheet. Ain Shams Engineering Journal 5: 1337-1342. https://doi.org/10.1016/j.asej.2014.06.002

[15] Hayat T, Asad S, Mustafa M, Alsaedi A. (2014). Radiation effects on the flow of Powell Eyring fluid past an unsteady inclined stretching sheet with non-uniform Heat Source/Sink. PLOS ONE 9(7): e103214. https://doi.org/10.1371/journal. pone. 0103214

[16] Darji RM, Timol MG. (2013). Group-theoretic similarity analysis for natural convection boundary layer flow of a class of non-newtonian fluids. International Journal of Advanced Scientific and Technical Research 3(1): 54-69.

[17] Gbadeyan JA, Dada MS. (2013). On the Influence of radiation radiation and heat transfer on an unsteady MHD Non-Newtonian fluid flow with slip in a porous medium. Journal of Mathematical Research 5(3): 40-49. http://dx.doi.org/10.5539/jmr.v5n3p40

[18] Oyelami FH, Dada MS. (2016). Unsteady magnetohydrodynamic flow of some non-Newtonian fluids with slip in a porous channel. International Journal of Heat and Technology 36(2): 709-713. https://doi.org/10.18280/ijht.360237

[19] Parmar A., Jain S. (2018). MHD Powell-Eyring fluid flow with non-linear radiation and variable thermal conductivity over a permeable cylinder. International Journal of Heat and Technology 36(1): 56-64. https://doi.org/10.18280/ijht

[20] Modest MF. (1993). Radiation heat transfer. Mac Graw-Hill, New York.

[21] Rapits A, Perdikis C. (2004). Unsteady flow through a highly porous medium in the presence of radiation. Transport Porous Media 57(2): 171-179. https://doi.org/10.1023/B:TIPM.0000038262.65594.e8

NOMENCLATURE

t^*	Dimensional time
t	Non-dimensional time
x^*, y^*	Dimensional coordinates along and normal to the plate
u^*, v^*	Dimensional velocities in $x^*$and y^* directions
g	gravitational acceleration
k	permeability
u	Velocity in the x direction
v	Velocity in the y direction
N	Thermal radiation parameter
P^*	Dimensional pressure
P	Non-dimensional fluid pressure
X, Y	Non-dimensional coordinate along and normal to the plate
U, V	Non-dimensional velocities in X and Y directions
N	Thermal radiation parameter
P^*	Dimensional pressure
P	Dimensionless fluid pressure
T^*	Dimensional temperature of fluid
T	Dimensionless temperature of fluid
C^*	Dimensional concentration of fluid
C	Non-dimensional concentration of fluid
A, F	Eyring-Powell parameters
B_0	Applied magnetic field
C_p	specific heat at constant pressure
D_a	Darcy number
E_c	Eckert number
G_r	Thermal Grashof number
P_r	Prandtl number
q_r	radiative heat flux
R_e	Reynolds number
T_w	Temperature of the plate
C_w	Concentration of the plate

Greek alphabets

ρ	density
σ	Stefan-Boltzmann constant
a, c	characteristic of Eyring-Powell model
μ	Viscosity
τ_{xy}	stress tensor
β_T and β_C	thermal volumetric coefficient and concentration volumetric coefficient